Anal. Chem. **2010,** *82,* 3547–3555

Design and Implementation of Electrochemical Cytosensor for Evaluation of Cell Surface Carbohydrate and Glycoprotein

Jing-Jing Zhang, Fang-Fang Cheng, Ting-Ting Zheng, and Jun-Jie Zhu*

Key Laboratory of Analytical Chemistry for Life Science (Ministry of Education of China), School of Chemistry and Chemical Engineering, Nanjing University, Nanjing 210093, P. R. China

A new strategy for assessing cell surface carbohydrates and P-glycoprotein (P-gp) expression status and quantifying the cell numbers with an electrochemical immunoassay was designed. In order to construct the base of the cytosensor, a novel 3-D architecture was initially fabricated by combining nitrogen-doped carbon nanotubes, thionine, and gold nanoparticles via a simple layer-by-layer method. The formed architecture provided an effective matrix for concanavalin A (Con A) binding and made the immobilized Con A hold high stability and bioactivity. On the basis of the specific recognition of cell surface mannosyl groups to Con A, the Con A/3-D architecture interface showed a predominant capability for cell capture. With another coupled signal amplification based on a enzymatic catalytic reaction of HRP toward the oxidation of thionine by the H_2O_2, which was induced by two-step immunoreactions, the proposed cytosensor showed an excellent analytical performance for the detection of HeLa cells ranging from 8.0×10^2 to 2.0×10^7 cells mL^{-1} with a limit of detection of 500 cells mL^{-1}. Moreover, with the use of preblocking procedures, the mannosyl groups and P-gp on single HeLa cell could be further detected to be $(4 \pm 2) \times 10^{10}$ molecules of mannose moieties and 8.47×10^6 molecules of P-gp. This strategy offers great promise for sensitive detection of cancer cells and cell surface receptors and thus may help improve cancer diagnosis and treatment.

As is well-known, early detection of cancer greatly increases the chances for successful treatment. Consequently, the research of accurate and sensitive recognition and detection of cancer cells is extremely important for cancer diagnosis and therapy. Current typical methods for the routine detection of cancer cells include immunohistochemistry, polymerase chain reaction (PCR), and flow cytometry.[1−3] Although they have a high detection rate, they usually require time-consuming labeling processes, qualified personnel, and stringent laboratory conditions, besides instrumentation and cost. Therefore, in recent years, there have been some attempts for cell detection using electrochemical biosensors,[4−6] which offer the advantages of high sensitivity, simplicity, rapid response, compatibility with miniaturization technology, and low cost. However, the selectivity of most electrochemical biosensors is limited, and hence, sensitive and valuable biomarkers for selective recognition and capture of target cancer cells are desirable.

Cell surface carbohydrates are attractive targets, which play important roles in cancer development and metastasis.[7−9] They are cell-type specific, and the expression profiles are distinct during cell growth and differentiation processes.[10] More importantly, changes in the expression of cell surface carbohydrates are often associated with a variety of diseases, especially cancers.[11,12] Thus, effective tools for the identification of cell surface carbohydrate expression patterns are desirable not only for understanding their roles in disease development but also for early diagnosis. Many methods have been developed for carbohydrates detection, including isothermal titration calorimetry (ITC),[13] mass spectrometry,[14] nuclear magnetic resonance,[15] Western blotting,[16] and affinity chromatography.[17] Although these approaches have been successful for their specific systems, most of them, unfortunately, either are time-consuming and labor-intensive or require highly technical expertise and sophisticated instrumentation. Inspired by

* To whom correspondence should be addressed. Tel&Fax: +86-25-83594976. E-mail: jjzhu@nju.edu.cn.

(1) Singh, S. K.; Hawkins, C.; Clarke, I. D.; Squire, J. A.; Bayani, J.; Hide, T.; Henkelman, R. M.; Cusimano, M. D.; Dirks, P. B. *Nature* **2004**, *432*, 396–401.
(2) Schamhart, D.; Swinnen, J.; Kurth, K. H.; Westerhof, A.; Kuster, R.; Borchers, H.; Sternberg, C. *Clin. Chem.* **2003**, *49*, 1458–1466.
(3) Phillips, J. A.; Xu, Y.; Xia, Z.; Fan, Z. H.; Tan, W. H. *Anal. Chem.* **2009**, *81*, 1033–1039.
(4) Jia, X. E.; Tan, L.; Zhou, Y. P.; Jia, X. F.; Xie, Q. J.; Tang, H.; Yao, S. Z. *Electrochem. Commun.* **2009**, *11*, 141–144.
(5) He, F.; Shen, Q.; Jiang, H.; Zhou, J.; Cheng, J.; Guo, D. D.; Li, Q. N.; Wang, X. M.; Fu, D. G.; Chen, B. A. *Talanta* **2009**, *77*, 1009–1014.
(6) Ding, L.; Ji, Q. J.; Qian, R. C.; Cheng, W.; Ju, H. X. *Anal. Chem.* **2010**, *82*, 1292–1298.
(7) Gorelik, E.; Galili, U.; Raz, A. *Cancer Metast. Rev.* **2001**, *20*, 245–277.
(8) Sacchettini, J. C.; Baum, L. G.; Brewer, C. F. *Biochemistry* **2001**, *40*, 3009–3015.
(9) Ohtsubo, K.; Marth, J. D. *Cell* **2006**, *126*, 855–867.
(10) Zhao, J.; Patwa, T. H.; Qiu, W. L.; Shedden, K.; Hinderer, R.; Misek, D. E.; Anderson, M. A.; Simeone, D. M.; Lubman, D. M. *J. Proteome Res.* **2007**, *6*, 1864–1874.
(11) Dube, D. H.; Bertozzi, C. R. *Nat. Rev. Drug Discovery* **2005**, *4*, 477–488.
(12) Ding, L.; Cheng, W.; Wang, X. J.; Ding, S. J.; Ju, H. X. *J. Am. Chem. Soc.* **2008**, *130*, 7224–7225.
(13) Dam, T. K.; Brewer, C. F. *Chem. Rev.* **2002**, *102*, 387–429.
(14) Zamfir, A.; Vakhrushev, S.; Sterling, A.; Niebel, H. J.; Allen, M.; Peter-Katalinic, J. *Anal. Chem.* **2004**, *76*, 2046–2054.
(15) Haiber, S.; Herzog, H.; Burba, P.; Gosciniak, B.; Lambert, J. *Fresenius J. Anal. Chem.* **2001**, *369*, 457–460.
(16) Oda, Y.; Sanders, J.; Roberts, S.; Maruyama, M.; Kiddie, A.; Furmanik, J.; Smith, B. R. *J. Clin. Endocrinol. Metab.* **1999**, *84*, 2119–2125.
(17) Casas-Solvas, J. M.; Ortiz-Salmeron, E.; Gimenez-Martinez, J. J.; Garcia-Fuentes, L.; Capitan-Vallvey, L. F.; Santoyo-Gonzalez, F.; Vargas-Berenguel, A. *Chem.—Eur. J.* **2009**, *15*, 710–725.

10.1021/ac9026127
Published on Web 04/06/2010

the concept of DNA and protein microarrays, lectin microarrays have been recently introduced as a glycan profiling tool in carbohydrates detection.[18−21] These microarrays mainly rely on the highly specific binding affinities between lectins and corresponding carbohydrate residues. In this respect, the majority of the detection protocols are based on labeled lectins or carbohydrates with a fluorescent moiety, which could induce a measurable signal. However, some disadvantages such as quenching phenomena and photochemical instability still exist in the process of detection. Instead, because of its inherent advantages, the electrochemical technique provides an elegant way for interfacing biorecognition events and signal transduction.[22−24]

On the other hand, the principal obstacle to effective chemotherapy of cancer is the fact of tumor cells exhibiting resistance to a broad spectrum of structurally diverse chemotherapeutic drugs, a phenomenon termed multidrug resistance (MDR).[25] One cause of MDR is the overexpression of an energy-dependent transport protein named P-glycoprotein (P-gp) at the tumor cell surface.[26] P-gp has a molecular weight of 170 kDa and comprises two nucleotide-binding and two membrane-spanning domains. It acts as an energy-dependent pump that reduces intracellular drug concentrations below therapeutically effective levels.[27] Accordingly, the ability to characterize cell surface glycoprotein expression status is critical to advance chemotherapy of the malignant tumor. In view of the above challenges, researchers attempted to develop effective protocols for detection of P-gp on the tumor cell surface.[28,29] These methods usually used an enzyme-linked immunoassay followed by an electrochemical or optical detection procedure. Although promising, these techniques are still the development phase because of the complexity of the immune recognition process on the cell surface. In view of the importance of cell surface carbohydrates and P-glycoprotein, a reliable and convenient method for assessing their expression status may help improve the diagnosis and treatment of cancer.

Carbon-based nanomaterials, especially carbon nanotubes (CNTs), have recently attracted considerable interest in constructing electrochemical biosensors because of their numerous signal amplifications and excellent electrocatalytic effects.[30−32] However, the pristine CNTs have complete graphene structures and relatively less defect sites, which results in some limitations to CNTs in the solubility, biocompatibility, and electrochemically contact with biomacromolecules. Considerable efforts have been made worldwide to circumvent these drawbacks, in which the doping CNTs with nitrogen atoms has been regarded as an effective and efficient strategy capable of introducing many defective sites on the nanotube surface.[33−35] Compared to undoped CNTs, nitrogen-doped carbon nanotubes (CN_X) have much larger functional surface area, higher ratio of surface active groups to volume, more biocompatible C−N microenvironment, and higher electrical conductivity. On the basis of these advantages, CN_X have been widely used in supercapacitors, fuel cells, and photosensing and enzyme biosensors.[36−38] However, to the best of our knowledge, only a few studies of the use of CN_X in electrochemical biosensors have been reported.[39,40] Such limited attention is not consistent with the remarkable properties and potential merits of CN_X.

The aim of the present investigation was to design a novel electrochemical cytosensing platform for cancer cell detection and also evaluation of cell surface carbohydrates and P-glycoprotein expression status. To this purpose, we first fabricated a 3-D architecture by combining CN_X, thionine (TH^+), and gold nanoparticles (AuNPs) via the layer-by-layer method. Because of the good biocompatibility of AuNPs and excellent conductivity of CN_X, the 3-D architecture not only provided a highly suitable microenvironment for lectins binding but also played a role of signal amplification in following electrochemical detection. Here, concanavalin A (Con A) was used as a model lectin, which could specifically recognize cell surface mannosyl groups. The conductive Con A/3-D architecture interface showed an excellent capability for cell capture, producing a sensitive sensor for cancer cell detection. Moreover, two-step immunoreactions based on the specific binding between the P-glycoprotein antibody and P-glycoprotein on the captured cell surface were further implemented, which could introduce further signal amplification based on the enzymatic catalytic reaction of HRP toward the oxidation of thionine by H_2O_2. The immunoassay procedure was shown in Scheme 1. The performance and factors influencing the performance of the electrochemical cytosensor were investigated. In addition, a method for evaluating the expression status of mannosyl groups and P-gp was also proposed based on preblocking the mannose or P-gp binding sites. Therefore, our approach not only exhibited attractive performances in cytosensing but also presented a significant tool

(18) Zheng, T.; Peelen, D.; Smith, L. M. *J. Am. Chem. Soc.* **2005**, *127*, 9982–9983.
(19) Koshi, Y.; Nakata, E.; Yamane, H.; Hamachi, I. *J. Am. Chem. Soc.* **2006**, *128*, 10413–10422.
(20) Simeone, D. M.; Lubman, D. M. *Anal. Chem.* **2006**, *78*, 6411–6421.
(21) Gao, J. Q.; Liu, D. J.; Wang, Z. X. *Anal. Chem.* **2008**, *80*, 8822–8827.
(22) Oliveira, M. D. L.; Correia, M. T. S.; Coelho, L. C. B. B.; Diniz, F. B. *Colloids Surf., B* **2008**, *66*, 13–19.
(23) Cheng, W.; Ding, L.; Lei, J. P.; Ding, S. J.; Ju, H. X. *Anal. Chem.* **2008**, *80*, 3867–3872.
(24) Dai, Z.; Kawde, A. N.; Xiang, Y.; La Belle, J. T.; Gerlach, J.; Bhavanandan, V. P.; Joshi, L.; Wang, J. *J. Am. Chem. Soc.* **2006**, *128*, 10018–10019.
(25) Hrycyna, C. A.; Ramachandra, M.; Germann, U. A.; Cheng, P. W.; Pastan, I.; Gottesman, M. M. *Biochemistry* **1999**, *38*, 13887–13899.
(26) Varma, M. V. S.; Sateesh, K.; Panchagnula, R. *Mol. Pharm.* **2004**, *2*, 12–21.
(27) Eckford, P. D. W.; Sharom, F. J. *Biochemistry* **2008**, *47*, 13686–13698.
(28) Du, D.; Ju, H. X.; Zhang, X. J.; Chen, J.; Cai, J.; Chen, H. Y. *Biochemistry* **2005**, *44*, 11539–11545.
(29) Shao, M. L.; Bai, H. J.; Gou, H. L.; Xu, J. J.; Chen, H. Y. *Langmuir* **2009**, *25*, 3089–3095.
(30) Liu, Q.; Lu, X. B.; Li, J.; Yao, X.; Li, J. H. *Biosens. Bioelectron.* **2007**, *22*, 3203–3209.
(31) Meng, L.; Jin, J.; Yang, G. X.; Lu, T. H.; Zhang, H.; Cai, C. X. *Anal. Chem.* **2009**, *81*, 7271–7280.
(32) Zhou, N.; Yang, T.; Jiang, C.; Du, M.; Jiao, K. *Talanta* **2009**, *77*, 1021–1026.
(33) Lepro, X.; Vega-Cantu, Y.; Rodriguez-Macia, F. J.; Bando, Y.; Golberg, D.; Terrones, M. *Nano Lett.* **2007**, *7*, 2220–2226.
(34) Yue, B.; Ma, Y. W.; Tao, H. S.; Yu, L. S.; Jian, G. Q.; Wang, X. Z.; Wang, X. S.; Lu, Y. N.; Hu, Z. *J. Mater. Chem.* **2008**, *18*, 1747–1750.
(35) Xiong, Y. J.; Li, Z. Q.; Guo, Q. X.; Xie, Y. *Inorg. Chem.* **2005**, *44*, 6506–6508.
(36) Fan, W. C.; Chyan, O.; Sun, C. L.; Wu, C. T.; Cheng, C. P.; Chen, K. H.; Chen, L. C.; Huang, J. H. *Electrochem. Commun.* **2007**, *9*, 239–244.
(37) Gong, K. P.; Du, F.; Xia, Z. H.; Durstock, M.; Da, L. M. *Science* **2009**, *323*, 760–764.
(38) Xiao, K.; Fu, Y.; Liu, Y. Q.; Yu, G.; Zhai, J.; Jiang, L.; Hu, W. P.; Shuai, Z. G.; Luo, Y.; Zhu, D. B. *Adv. Funct. Mater.* **2007**, *17*, 2842–2846.
(39) Jia, N. Q.; Liu, L.; Zhou, Q.; Wang, L. J.; Yan, M. M.; Jiang, Z. Y. *Electrochim. Acta* **2005**, *51*, 611–618.
(40) Jia, N. Q.; Wang, L. J.; Liu, L.; Zhou, Q.; Jiang, Z. Y. *Electrochem. Commun.* **2005**, *7*, 349–354.

Scheme 1. Schematic Representation of the Fabrication of the Cell-Based Electrochemical Enzyme-Linked Immunoassay

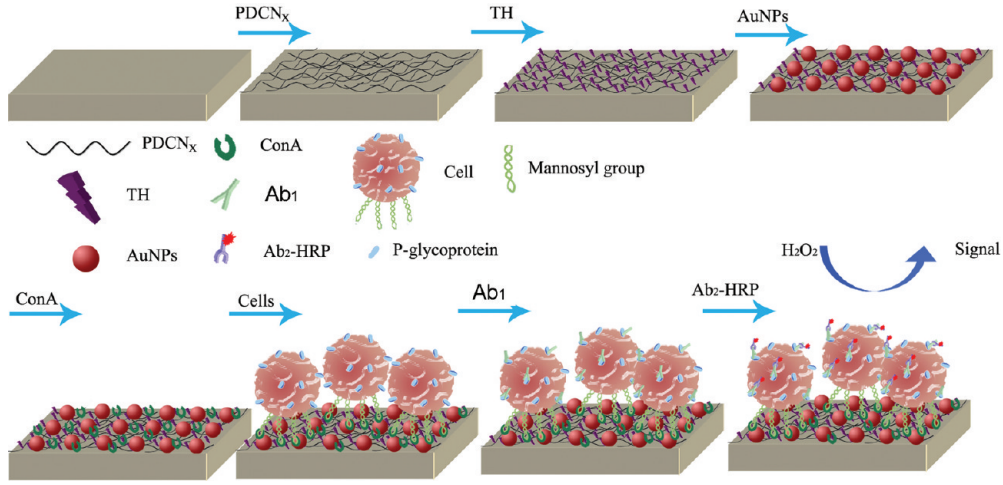

for evaluation of cell surface carbohydrates and P-glycoprotein, suggesting potential applications in cancer diagnosis.

EXPERIMENTAL SECTION

Materials and Reagents. Concanavalin A and poly(diallyldimethylammonium chloride) (PDDA, 20%, w/w in water, MW = 200 000−350 000) were purchased from Sigma-Aldrich. Chloroauric acid ($HAuCl_4 \cdot 4H_2O$) and trisodium citrate were obtained from Shanghai Chemical Reagent Co. (Shanghai, China). P-gp mouse monoclonal antibody (Ab_1, 200 μg mL^{-1}) and the secondary antibody of HRP-labeled goat antimouse (Ab_2-HRP, 2 mg mL^{-1}) were purchased from Wuhan Boster Biological Technology Co. Ltd. (Wuhan, China). Thionine chloride (TH^+) was purchased from Sinopharm Chemical Reagent Co. Ltd. (Shanghai, China). Analytical grade mannose was from Sinopharm Chemical Reagent Co. Ltd. (China). Nitrogen-doped multiwalled carbon nanotubes (CN_X nanotubes) with a nitrogen content of 3.2%, prepared as described in ref 28. AuNPs were prepared according to the literature by adding a sodium citrate solution to a boiling $HAuCl_4$ solution.[41] Phosphate buffer saline (PBS, pH 7.4) contained 137 mM NaCl, 2.7 mM KCl, 87 mM Na_2HPO_4, and 14 mM KH_2PO_4. All other reagents were of analytical grade. All aqueous solutions were prepared using ultrapure water (Milli-Q, Millipore).

CN_X of a certain mass were dispersed in a mixture of sulfuric acid and nitric acid (3:1) and sonicated for about 3 h to obtain carboxylic group-functionalized CN_X. After centrifugation from the mixture, the sediment was washed repeatedly with distilled water until the pH reached 7.0. The oxidized CN_X were further functionalized with PDDA according to the reported method except that CN_X were used instead of CNTs.[42] The collected PDDA-functionalized CN_X ($PDCN_X$) was redispersed in water to a concentration of 5.0 mg mL^{-1}.

Cell Line and Culture. The HeLa cells obtained from a human epithelial carcinoma cell line were cultured in a flask in RPMI 1640 medium (Gibco, Grand Island, NY) supplemented with 10% fetal calf serum (FCS, Sigma), penicillin (100 μg mL^{-1}), and streptomycin (100 μg mL^{-1}) in an incubator (5% CO_2, 37 °C). At the logarithmic growth phase, the cells were trypsinized and washed twice with sterile pH 7.4 PBS by centrifugation at 1000 rpm for 10 min. The sediment was then resuspended in 0.1 M pH 7.4 PBS containing 1 mM Ca^{2+} and 1 mM Mn^{2+} to obtain a homogeneous cell suspension. The cell number was determined using a Petroff-Hausser cell counter.

Electrode Preparation and Cell Capture. A glass carbon electrode (GCE) was successively polished to a mirror by using 0.3 and 0.05 μm alumina slurry (Beuhler) followed by rinsing thoroughly with water. After successive sonication in 1:1 nitric acid/water, acetone, and doubly distilled water, the electrode was rinsed with doubly distilled water and allowed to dry at room temperature. As shown in Scheme 1, 5 μL of 5.0 mg mL^{-1} $PDCN_X$ solution was first dropped on the pretreated GCE and dried in a silica gel desiccator and then immersed in 5 mM thionine solution for 30 min. After a thorough rinse with deionized water, the electrode was subsequently immersed into an AuNPs solution for 1 h to yield an AuNPs/TH^+/$PDCN_X$ modified GCE. The immobilization of Con A was accomplished by dropping 5 μL of 4 mg mL^{-1} Con A solution on the AuNPs/TH^+/$PDCN_X$ surface. The electrode was incubated at 4 °C for at least 24 h in a moisture atmosphere to avoid evaporation of solvent, following a carefully rinse with 0.1 M pH 7.4 PBS to remove physically absorbed protein. After that, the electrode was soaked in 20 μL of HeLa cell suspension at a certain concentration and incubated at 37 °C for 2 h to capture the cells via the specific binding between Con A and cell surface mannosyl group. Then the electrode was taken out and carefully rinsed with pH 7.4 PBS to remove the noncaptured cells. The obtained HeLa/Con A/AuNPs/TH^+/$PDCN_X$/GCE was used for subsequent immunoassay.

Enzyme-Amplified Electrochemical Immunoassay. The HeLa/Con A/AuNPs/TH^+/$PDCN_X$/GCE was first incubated with 10 μg mL^{-1} Ab_1 and then with 10 μg mL^{-1} Ab_2-HRP at 37 °C for 60 min, respectively. Finally, the electrode was washed thoroughly with pH 7.4 PBS to remove nonspecifically bound conjugates to minimize the background response. The electrochemical measurement was performed in degassed 0.1 M pH 7.4 PBS containing 10 mM H_2O_2. The differential pulse voltammetry (DPV) measurements were performed from −0.5 to 0 V with a pulse amplitude of 50 mV and width of 0.2 s.

(41) Zhang, S. S.; Zhong, H.; Ding, C. F. *Anal. Chem.* **2008**, *80*, 7206–7212.
(42) Cui, R. J.; Liu, C.; Shen, J. M.; Zhu, J. J.; Chen, H. Y. *Adv. Funct. Mater.* **2008**, *18*, 2197–2204.

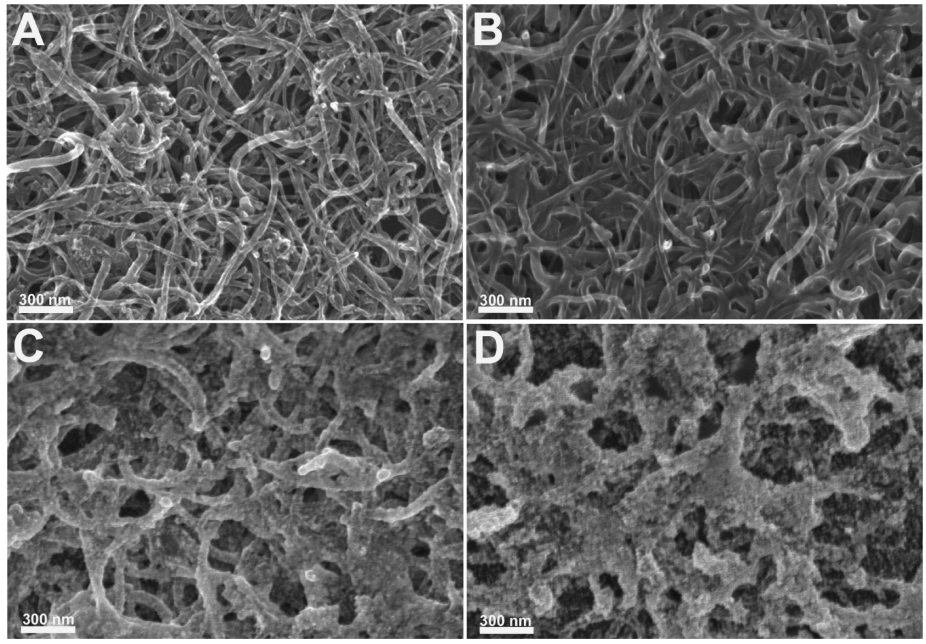

Figure 1. Representative FESEM images of $PDCN_X$/GCE (A), $TH^+/PDCN_X$/GCE (B), AuNPs/$TH^+/PDCN_X$/GCE (C), and Con A/AuNPs/$TH^+/PDCN_X$/GCE (D).

Apparatus. Scanning electron micrographs (SEM) were obtained with a Hitachi S4800 scanning electron microscope. Transmission electron micrographs (TEM) were measured on a JEOLJEM 200CX transmission electron microscope using an accelerating voltage of 200 kV. X-ray photoelectron spectroscopy (XPS) was carried out on an ESCALAB MK II X-ray photoelectron spectrometer. The static water contact angles were measured at 25 °C by a contact angle meter (Rame-Hart-100) employing drops of pure deionized water. The readings were stabilized and taken within 120 s after the addition. Electrochemical measurements were performed on a CHI 660c workstation (Shanghai Chenhua Apparatus Corporation, China) with a conventional three-electrode system comprised of a platinum wire as the auxiliary, a saturated calomel electrode as the reference, and the modified GCE as the working electrode. Electrochemical impedance spectroscopy (EIS) was performed with an Autolab electrochemical analyzer (Eco Chemie, The Netherlands) in a 10 mM $K_3Fe(CN)_6/K_4Fe(CN)_6$ (1:1) mixture with 1.0 M KCl as the supporting electrolyte, using an alternating current voltage of 5.0 mV, within the frequency range of 0.01 Hz−100 kHz.

RESULTS AND DISCUSSION

Characterization of the Modified Electrodes. It is well-known that the surface-modified technology could present some superior response performances to the analytes.[43] Herein, we tried to fabricate an improved interface using nitrogen-doped carbon nanotubes (CN_X) and gold nanoparticles (AuNPs) for the immobilization of Con A. Figure S1 in the Supporting Information showed the typical TEM image of the CN_X. It can be seen that the pristine CN_X displayed a bamboo-shaped structure containing highly oriented multiwalled nanotubes of uniform diameter (~10−30 nm). XPS was employed to further confirm the existence of nitrogen in the nanotubes. As shown in Figure S2 in the Supporting Information, the XPS survey scan spectrum exhibited distinct C 1s, N 1s, and O 1s peaks. The N 1s XPS spectrum for CN_X showed three bands at about 399.5, 401.1, and 404.4 eV, corresponding to the "pyrrolic", "pyridinic" nitrogen incorporation within the grapheme sheets and nitrogen atoms substituting inner carbon atoms in the interior, respectively.[44] The N content for the CN_X was detected to be about 3.2%. In order to increase the solubility and biocompatibility of nanotubes, CN_X were initially acid-oxidized to introduce carboxyl groups on the surface of the carbon nanotubes, followed by being functionalized with a cationic polyelectrolyte (PDDA). Then, because of the unique interaction between NH_2-terminated thionine and $PDCN_X$, the thionine molecules could be firmly absorbed onto $PDCN_X$-modified electrode. Subsequently, AuNPs could be further electrostatic absorbed to the $TH^+/PDCN_X$ modified surface. Finally, Con A was immobilized onto the AuNPs because of the strong interaction between AuNPs and the primary amine groups in the biomolecules.[22,45,56]

SEM was used to characterize the stepwise fabrication process of the immunosensor. As shown in Figure 1A, the $PDCN_X$ film displayed a well-dispersed one-dimensional structure in the form of small bundles or single tubes. The diameters of these bundles were 15−30 nm. As compared with the image of the $PDCN_X$ film, the more dense and homogeneous structure could be observed for the $TH^+/PDCN_X$ film (Figure 1B), indicating the binding of thionine onto the $PDCN_X$ surface. The SEM image of AuNPs/$TH^+/PDCN_X$ in Figure 1C exhibited that numerous gold nanoparticles were decorated onto the $TH^+/PDCN_X$ film quite uniformly through the opposite-charged adsorption and the interaction with the amino groups of Th^+. It should be mentioned that the positively charged PDDA may also play a role in the attachment

(43) Murphy, L. *Curr. Opin. Chem. Biol.* **2006**, *10*, 177–184.

(44) Maldonado, S.; Stevenson, K. J. *J. Phys. Chem. B* **2005**, *109*, 4707–4716.

(45) Labib, M.; Hedstrom, M.; Amin, M.; Mattiasson, B. *Anal. Chim. Acta* **2010**, *659*, 194–200.

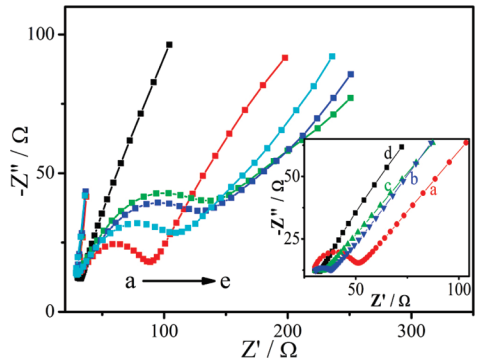

Figure 2. Nyquist diagrams of electrochemical impedance spectra recorded from 0.1 to 10^6 Hz for $[Fe(CN)_6]^{3-}/[Fe(CN)_6]^{4-}$ (10 mM, 1:1) in 1.0 M KCl at a Con A/AuNPs/TH^+/$PDCN_X$/GCE (a), HeLa/Con A/AuNPs/TH^+/$PDCN_X$/GCE (b), Ab_1/HeLa/Con A/AuNPs/TH^+/$PDCN_X$/GCE (c), and Ab_2-HRP/Ab_1/HeLa/Con A/AuNPs/TH^+/$PDCN_X$/GCE (d). The inset is the EIS of bare GCE (a), $PDCN_X$/GCE (b), TH^+/$PDCN_X$/GCE (c), and AuNPs/TH^+/$PDCN_X$/GCE (d).

of AuNPs to the TH^+/$PDCN_X$ surface. This uniform nanostructure provided a significant increase of the effective electrode surface for loading of biomolecules and accelerating electron transfer. After immersion in Con A solution for 24 h, the surface became much rougher and richer in texture (Figure 1D) due to the aggregation of Con A. Because of the porous structure and the excellent properties of the AuNPs doped TH^+/$PDCN_X$ membrane, it retained the bioactivity of Con A to produce a good analytical performance of the immunosensors.

The hydrophilicity of an electrode surface is commonly used to characterize its biocompatibility, which could be measured with the contact angle of the substrate. As shown in Figure S3 in the Supporting Information, the contact angles of the $PDCN_X$, TH^+/$PDCN_X$, and AuNPs/TH^+/$PDCN_X$ were 32.6°, 31.6°, and 22.4°, respectively. The AuNPs/TH^+/$PDCN_X$ film showed the lowest contact angle, indicating better hydrophilicity, which may be attributed to the multiple defects from nitrogen doping and more carboxylate groups produced by the acidic treatment process. Thus, the improved biocompatibility of the AuNPs/TH^+/$PDCN_X$ film was in favor of enhancing protein loading and retaining the bioactivity.

As a powerful tool for probing the interface features of surface-modified electrodes, EIS was further used to study the stepwise assembly of the immunosensor. The impedance spectra include a semicircle portion and a linear portion. The semicircle portion at higher frequencies corresponds to the electron-transfer limited process, and the linear portion at lower frequencies represents the diffusion-limited process. The semicircle diameter equals the electron-transfer resistance (R_{et}). Figure 2 illustrates the Nyquist plots of EIS for the different modified electrodes in presence of redox probe, $Fe(CN)_6^{4-/3-}$. At a bare GCE, the redox process of the probe showed an electron-transfer resistance of about 38.5 Ω (curve a, inset of Figure 2), while the $PDCN_X$-modified electrode showed a lower resistance for the redox probe (curve b, inset of Figure 2), implying that $PDCN_X$ was an excellent electric conducting material and accelerated electron transfer. In the cases of TH^+/$PDCN_X$/GCE and AuNPs/TH^+/$PDCN_X$/GCE (curves c and d, inset of Figure 2), the resistance further decreased because of the contribution of assembled TH^+ and AuNPs. When Con A was assembled on the AuNPs/TH^+/$PDCN_X$/GCE, the resistance increased greatly (curve a in Figure 2), suggesting that Con A molecules were immobilized on the electrode and blocked the electron exchange between the redox probe and the electrode. The results were consistent with the observation from FESEM images as shown in Figure 1. Subsequently, after the capture of cancer cells, the R_{et} increased again (curve b in Figure 2), owing to the dielectric behavior of cells for interfacial electron transfer processes. Additionally, the access of the redox probe to the electrode surface would further be hindered after incubation with Ab_1 and then the Ab_2-HRP (curves c and d in Figure 2), due to the resistance of proteins, causing a further increase of R_{et}. Thus, we might conclude that the AuNPs/TH^+/$PDCN_X$ composite film not only offered a biocompatible surface for protein loading and cell capture but also provided a sensitive electric interface for further sensing.

Electrochemical Characteristics of Cell-Based Immunoassay. As shown in Figure 3A, no detectable cyclic voltammetric response was observed for the bare GCE and the $PDCN_X$/GCE because of the lack of electron mediator. The latter displayed a larger background current due to the larger accessible surface area of the modified electrode.[46] After Th^+ was adsorbed onto the $PDCN_X$/GCE, the resulting electrode displayed a reversible, two-electron transfer process cyclic voltammogram with good stability and reproducibility (curve c), indicating the well electroactive performance of the Th^+ mediator. With a comparison between curves c and d in Figure 3A, the peak currents increased dramatically after the binding of AuNPs. The reason may be that nanometer-sized gold nanoparticles played an important role similar to a conducting wire or electron-conducting tunnel. However, the peak currents decreased after the modified electrode was immersed in the Con A solution (Figure 3B, curve a), which indicated that Con A had been immobilized on the electrode surface successfully. Subsequently, when the Con A/AuNPs/TH^+/$PDCN_X$/GCE was incubated with HeLa cells, a dramatic decrease of the peak currents may be attributed to the captured cells, which can hinder the transmission of electrons toward the electrode surface (Figure 3B, curve b). Then it should be noted that the peak currents further decreased slightly after the two-step immunoreactions (curves c and d, Figure 3B).

In order to evaluate the catalysis of the immobilized HRP to H_2O_2, we studied the cyclic voltammograms of Ab_2-HRP/Ab_1/HeLa/Con A/AuNPs/TH^+/$PDCN_X$/GCE in the absence and presence of H_2O_2. As shown in Figure 3C, the modified electrode exhibited a pair of stable and well-defined redox peaks at −0.161 and −0.366 V in pH 7.4 PBS (curve a), which corresponded to the redox reactions of the immobilized thionine. Also, both the anodic and cathodic peak currents were proportional to the scan rate in the range from 20 to 300 mV s^{-1}, indicating a surface-controlled electrode process. Upon addition of 10 mM H_2O_2 to the solution, the reduction peak current increased and the oxidation peak current decreased greatly (curve b), suggesting an obvious electrocatalytic process for the oxidation of thionine by the H_2O_2 at the immunosensor. However, the cytosensor

(46) Su, H. L.; Yuan, R.; Chai, Y. Q.; Zhuo, Y.; Hong, C. L.; Liu, Z. Y.; Yang, X. *Electrochim. Acta* **2009**, *54*, 4149–4154.

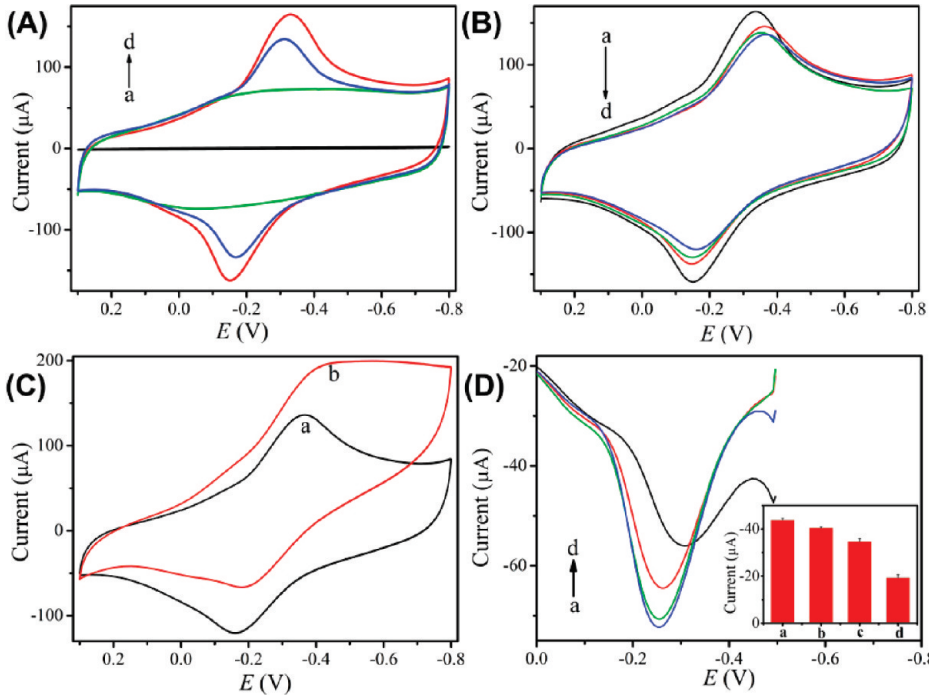

Figure 3. (A) Cyclic voltammograms of bare GCE (a), $PDCN_X$/GCE (b), TH^+/$PDCN_X$/GCE (c), and AuNPs/TH^+/$PDCN_X$/GCE (d) in 0.1 M pH 7.4 PBS. (B) Cyclic voltammograms of Con A/AuNPs/TH^+/$PDCN_X$/GCE (a), HeLa/Con A/AuNPs/TH^+/$PDCN_X$/GCE (b), Ab_1/HeLa/Con A/AuNPs/TH^+/$PDCN_X$/GCE (c), and Ab_2-HRP/Ab_1/HeLa/Con A/AuNPs/TH^+/$PDCN_X$/GCE (d) in 0.1 M pH 7.4 PBS. (C) Cyclic voltammograms of Ab_2-HRP/Ab_1/HeLa/Con A/AuNPs/TH^+/$PDCN_X$/GCE in 0.1 M pH 7.4 PBS containing no H_2O_2 (a) and 10 mM (b) H_2O_2, respectively. Scan rate: 100 mV s^{-1}. (D) DPV curves of HeLa/Con A/AuNPs/TH^+/$PDCN_X$/GCE (a), Ab_1/HeLa/Con A/AuNPs/TH^+/$PDCN_X$/GCE (b), and Ab_2-HRP/Ab_1/HeLa/Con A/AuNPs/TH^+/$PDCN_X$/GCE (c) in 0.1 M pH 7.4 PBS and Ab_2-HRP/Ab_1/HeLa/Con A/AuNPs/TH^+/$PDCN_X$/GCE in 0.1 M pH 7.4 PBS containing 10 mM H_2O_2 (d). Inset was the corresponding DPV peak currents of part D.

showed a very small catalytic oxidation current in the absence of Ab_2-HRP, indicating the catalytic efficiency of thionine to H_2O_2 was quite low (Figure S4 in the Supporting Information). Thus, HRP attached to the electrode surface has retained its catalytic activity and participated in the electrocatalytic reactions.

In comparison with other chronoamperometric or EIS protocols used in cell-based biosensor, the DPV technique has a potential advantage to increase the sensitivity and selectivity in the process of detection.[47] Figure 3D showed the DPV curves of the modified electrodes. It can be seen that the oxidation peak current decreased gradually during the two-step immunoreactions (curves a−c, Figure 3D). However, the oxidation peak current of Ab_2-HRP/Ab_1/HeLa/Con A/AuNPs/TH^+/$PDCN_X$/GCE showed a sharp decrease after the addition of 10 mM H_2O_2 to the solution. It may be attributed to the immobilized HRP which could catalyze the oxidation reaction of thionine by H_2O_2.[48] The detailed change of oxidation peak current could be seen from the inset of Figure 3D clearly. The decrease of the DPV peak current was directly related to the coverage of the immobilized HRP, which depended on both the amount of cells captured on the cytosensor surface and the expression of P-gp on the cell membrane. Moreover, as mentioned above, the HeLa cells were captured on the cytosensor surface via the specific binding between cell surface mannosyl groups and Con A. In other words, the amount of cells captured on the cytosensor surface was related to the expression of mannosyl groups on the cell surface. Thus, the expression of carbohydrate groups and glycoprotein could be evaluated by monitoring the enzyme amplified electrochemical signal.

Optimization of Experimental Conditions. The electrochemical performance of the cytosensor would be influenced by many factors. At the AuNPs/TH^+/$PDCN_X$/GCE, the electrochemical signal was related to the preparation process of the AuNPs-TH^+-$PDCN_X$ film. Herein, we investigated the dependence of the DPV peak current under different experimental variables, containing the concentration of $PDCN_X$, concentration of TH^+, and incubation time of AuNPs. As shown in Figure 4A, a significant increase of DPV peak current was observed between 0.5 and 5.0 mg mL^{-1}, while insignificant differences were obtained for greater concentrations. For convenience, 5.0 mg mL^{-1} of $PDCN_X$ was used for electrode modifications. Figure 4B showed the dependence of TH^+ concentration on the DPV peak current in pH 7.4 PBS. With the increasing concentration of TH^+, the DPV peak current increased and reached a maximum response at the TH^+ concentration of 5.0 mM. When the concentration of TH^+ was greater than 5.0 mM, the current decreased slightly to lead to the leakage of the excessive thionine molecules from the electrode surface. Meanwhile, the excessive thionine molecules were adverse to the adhesion of cells. Thus, the optimal concentration of TH^+ was 5.0 mM. Moreover, the amount of AuNPs bound to the electrode surface was an important parameter for both improving the conductivity of the sensing interface and the immobilization of Con A. With the incubation time increasing for AuNPs, the DPV peak current sharply increased and tended to a steady value after 60 min (Figure 4C), indicating a tendency of thorough attachment of AuNPs on the sensor. Longer incubation time did not enhance the response. Therefore, 60 min was chosen for the incubation of AuNPs. Under these conditions, the

(47) Liao, W. C.; Ho, J. A. A. *Anal. Chem.* **2009**, *81*, 2470–2476.
(48) Tang, D. P.; Yuan, R.; Chai, Y. Q. *Anal. Chem.* **2008**, *80*, 1582–1588.

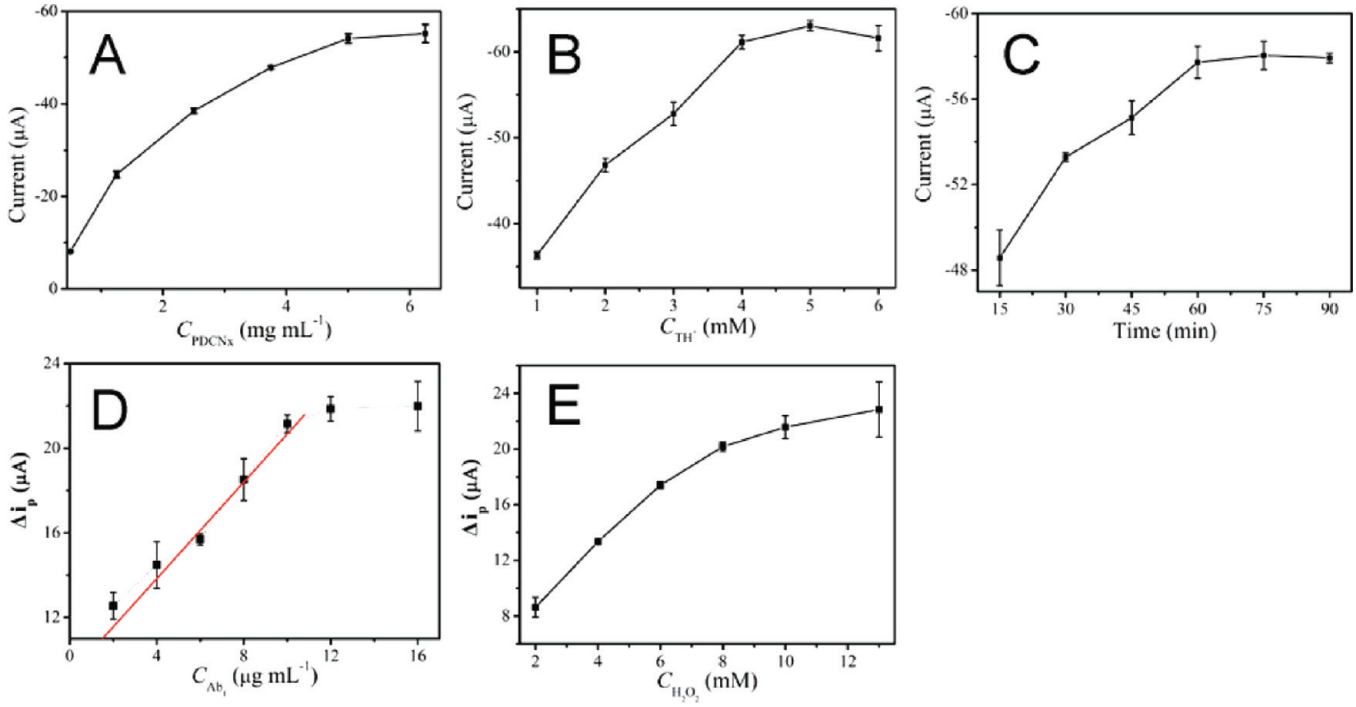

Figure 4. Effects of (A) concentration of $PDCN_X$, (B) concentration of TH^+, and (C) incubation time of AuNPs on the DPV peak currents of AuNPs/TH^+/$PDCN_X$ modified GCE in pH 7.4 PBS and dependence of the decrease of DPV peak currents of the enzyme-catalyzed analysis on Ab_1 concentration (D) and H_2O_2 concentration (E) in pH 7.4 PBS. When one parameter changes, the others are under their optimal conditions.

obtained AuNPs/TH^+/$PDCN_X$/GCE could offer a suitable interface with optimal biocompatibility and conductivity for Con A loading and cell capture, which thus increased the sensitivity of the cytosensor.

In addition, the amount of Ab_1 bounded to HeLa/Con A/AuNPs/TH^+/$PDCN_X$/GCE was also an important parameter for sensitive and reproducible immunoassay of P-gp on the cell membrane. Figure 4D showed the dependence of Ab_1 concentration in the incubation solution on the electrocatalytic peak current (Δi_p). Here the Δi_p value was defined as the difference between the oxidation DPV peak current before and after the addition of 10 mM H_2O_2 for the Ab_2-HRP/Ab_1/HeLa/Con A/AuNPs/TH^+/$PDCN_X$/GCE in pH 7.4 PBS. With the increasing concentration of Ab_1, the Δi_p values increased linearly and approached a constant value after 10.0 μg mL^{-1}. Thus, 10.0 μg mL^{-1} was used for the incubation.

The effect of H_2O_2 concentration in the electrochemical enzyme-catalyzed reaction was also examined as shown in Figure 4E. It can be seen that the Δi_p value increased when H_2O_2 concentrations were in the range from 2.0 to 10.0 mM, and then it started to level off and sometimes decreased slightly. The reason was the fact that the immobilized HRP was irreversibly transferred to its higher oxidized and inactive form at a higher H_2O_2 concentration.[49] Additionally, we also studied the stability of the cytosensor under 10.0 mM H_2O_2. As shown in Figure S5 in the Supporting Information, the cytosensor's response remained 85% of the original catalytic response after three continuous scans, showing acceptable stability. Therefore, 10.0 mM H_2O_2 was chosen for the test.

Detection of HeLa Cells. Comparing with the cell-based EIS-signaling system reported previously, we used an alternative differential pulse voltammetric (DPV) detection system with high sensitivity and short time for the detection of HeLa cells. The enzymatic catalytic signal was directly related to the amount of cells attached on the electrode surface. Figure 5A displayed the linear calibration plots of the electrocatalytic peak current (Δi_p) versus concentrations of the HeLa cells using the two-step immunoassay under optimal conditions. A linear relationship between the Δi_p value and logarithmic value of HeLa cells concentration could be found in the range of 8.0×10^2 to 2.0×10^7 cells mL^{-1}. The linear regression equation was Δi_p (μA) = $-3.37 + 4.34 \log C_{cells}$ (cells mL^{-1}) with a correlation coefficient of 0.993 ($n = 10$). The detection limit for cell concentration was estimated to be 500 cells mL^{-1} at 3σ, which was much lower than the detection limit recently reported by our group using a c-SWNTs-AuNPs-gelatin modified GCE with impedance measurements.[50]

The reproducibility of the cytosensor was evaluated from the DPV response of the Con A/AuNPs/TH^+/$PDCN_X$ modified electrode. A series of six measurements from the batch resulted in a relative standard deviation (RSD) of 4.2%, indicating good electrode-to-electrode reproducibility of the fabrication protocol described above. On the other hand, the intra-assay precision of the cytosensor was estimated by assaying two cell concentrations for six replicate measurements. At the cell concentrations of 5×10^5 and 2×10^6 cell mL^{-1}, the RSDs of intra-assay with this method were 6.2% and 6.6%, showing an acceptable precision. Since stability is a very important characteristic, it was necessary to check it for the developed cytosensor here. When the Con A/AuNPs/TH^+/$PDCN_X$ modified cytosensor was stored in the refrigerator at 4 °C, the DPV response was still retained at 90.3%

(49) Lu, X. B.; Wen, Z. H.; Li, J. H. *Biomaterials* **2006**, *27*, 5740–5747.

(50) Zhang, J. J.; Gu, M. M.; Zheng, T. T.; Zhu, J. J. *Anal. Chem.* **2009**, *81*, 6641–6648.

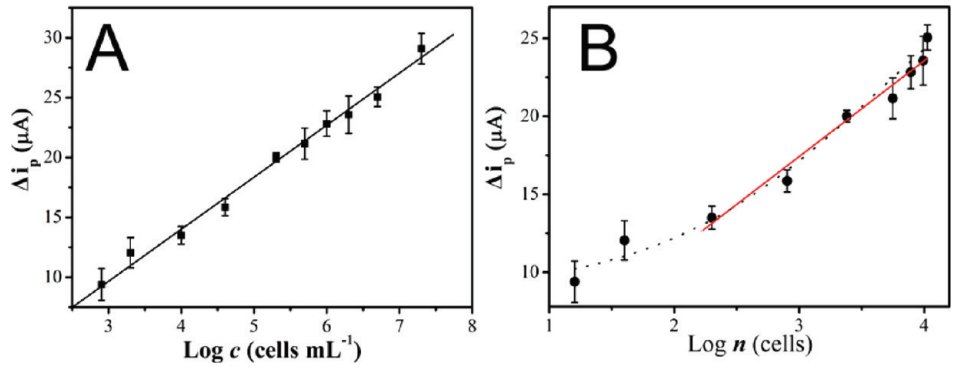

Figure 5. Calibration curve of the decrease of DPV peak current vs logarithm of the HeLa cell concentration (A) and number of captured HeLa cells on the cytosensor. The conditions are the same as in Figure 3D.

Table 1. Comparison of Analytical Performance of Some Cell-Based Biosensors

sensor fabrication[a]	cells[b]	linear range	detection limit	ref
interdigitated Au	*S. typhimurium*	10^5 to 10^9 cells mL^{-1}	10^5 cells mL^{-1}	51
Ab/MACA/Au	*E. coli*	3×10^3 to 3×10^7 cfu mL^{-1}	1×10^3 cfu mL^{-1}	52
PS/PANI/AuNPs/GCE	HL-60	1.6×10^3 to 1.6×10^8 cells mL^{-1}	730 cells mL^{-1}	53
aptamer/MCH/Au	CCRF-CEM	1×10^4 to 1×10^7 cells mL^{-1}	6×10^3 cells mL^{-1}	54
AuNPs/GCE	K562	5×10^4 to 10^7 cells mL^{-1}	500 cells	55
$PDCN_X$/TH^+/AuNPs/GCE	HeLa	8×10^2 to 2×10^7 cells mL^{-1}	500 cells mL^{-1}	this work

[a] Au, gold electrode; Ab, anti-*E. coli* antibody; MACA, mercaptoacetic acid; PS, polystyrene; PANI, polyaniline; MCH, 6-mercapto-1-hexanol. [b] *S. typhimurium*, *Salmonella typhimurium*; *E. coli*, *Escherichia coli*.

value of the initial response, showing a quite satisfying stability. Good stability can be attributed to the strong interactions between the AuNPs/TH^+/$PDCN_X$ and Con A.

Furthermore, the analytical performance of the developed cell sensor has been compared with those cell sensors reported in the literatures. Characteristics such as the linear range and detection limit are summarized for all of them in Table 1. As can be observed, the proposed sensor exhibit a wide linear range and low detection limit for cancer cells. The reasons might be as follows: first, because of the unique structural and electrical properties, the $PDCN_X$ could provide a larger specific surface area to adsorb Th^+ and promise abundant binding of AuNPs. Accordingly, by combination of the excellent conductivity of $PDCN_X$, good electronic media performance of TH^+, and outstanding biocompatibility of AuNPs, the novel architecture of AuNPs/TH^+/$PDCN_X$ was suitable for the immobilization of Con A with high stability and bioactivity, resulting in an ideal interface for cell capture and thus improved the sensitivity of the cell sensor. Second, the two-step immunoreaction would further enhance the sensitivity of the present strategy via the signal amplification of enzymatic catalysis. The introduction of HRP to the sensing interface induced the oxidation reaction of thionine by H_2O_2, leading to a remarkable change of current signal. Thus, the presented strategy could afford a simple and applicable way for cancer cell quantification with acceptable sensitivity, stability, and reproducibility.

Evaluation of Mannosyl Groups and P-Glycoprotein on the Cell Surface. In living systems, the specific carbohydrate−lectin recognition events govern many psychological and pathological processes, which hold great relevance for both drug discovery and biomaterials applications.[56] It is reported that Con A can specifically recognize mannose residues on the cell surface.[57] Thus, the proposed cytosensor was further used for quantitative evaluation of cell surface mannosyl groups. The enzymatic catalytic signal was directly related to the amount of immobilized HRP, which depended on the number of captured cells. Meanwhile, the number of captured cells on the cytosensor surface was associated with the expression of mannosyl groups on the cell surface. Namely, the electrochemical signal was indirectly related to the expression of mannosyl groups on the cell surface. Thus, a method was designed by partly blocking the mannose-specific binding sites of immobilized Con A with mannose solutions at different concentrations for 1 h. The resulting mannose/Con A/AuNPs/TH^+/$PDCN_X$/GCE was then used for the capture of cells. Because of the partly blocked mannose-specific binding sites, the number of captured cells would somewhat decrease, resulting in a lower enzymatic catalytic current compared to that obtained without blocking. For evaluating the amount of mannosyl groups on the cell surface, the dependence of Δi_p on the number of captured cells (n) on the cytosensor was first investigated. Here, the n value was defined as the difference between the original cell number for incubation and the free cell number in the

(51) Laczka, O.; Baldrich, E.; Munoz, F. X.; del Campo, F. J. *Anal. Chem.* **2008**, *80*, 7239–7247.
(52) Gang, P.; Zhang, X. N.; Meng, W. W.; Wang, Q. J.; Zhang, W.; Jin, L. T.; Feng, Z.; Wu, Z. R. *Electrochim. Acta* **2008**, *53*, 4663–4668.
(53) Gu, M. M.; Zhang, J. J.; Li, Y.; Jiang, L. P.; Zhu, J. J. *Talanta* **2009**, *80*, 246–249.
(54) Pan, C. F.; Guo, M. L.; Nie, Z.; Xiao, X. L.; Yao, S. Z. *Electroanalysis* **2009**, *21*, 1321–1326.
(55) Hua, H. L.; Jiang, H.; Wang, X. M.; Chen, B. A. *Electrochem. Commun.* **2008**, *10*, 1121–1124.
(56) Liang, C. H.; Wang, C. C.; Lin, Y. C.; Chen, C. H.; Wong, C. H.; Wu, C. Y. *Anal. Chem.* **2009**, *81*, 7750–7756.
(57) Lis, H.; Sharon, N. *Chem. Rev.* **1998**, *98*, 637–674.

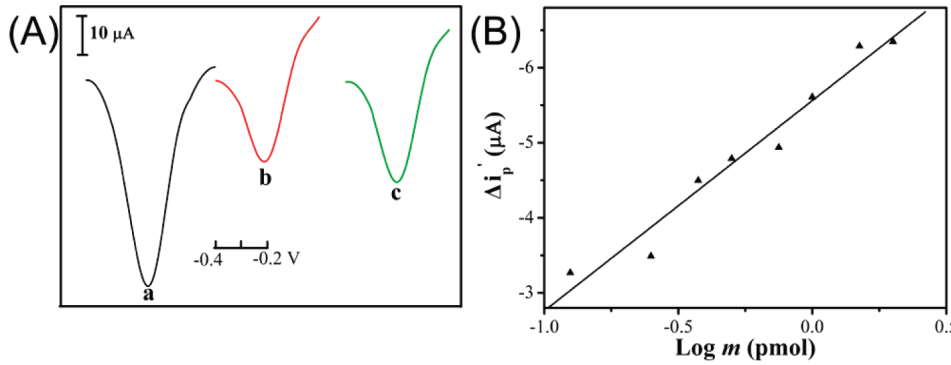

Figure 6. (A) DPV curves of Ab_2-HRP/Ab_1/HeLa/Con A/AuNPs/TH^+/$PDCN_X$/GCE (a) before and (b) after the addition of 10 mM H_2O_2 in 0.1 M pH 7.4 PBS, and (c) Ab_2-HRP/Ab_1/HeLa/Con A/AuNPs/TH^+/$PDCN_X$/GCE in 0.1 M pH 7.4 PBS containing 10 mM H_2O_2 after partly blocking Con A/AuNPs/TH^+/$PDCN_X$/GCE with mannose. (B) Effect of the amount of mannose used to block Con A/AuNPs/TH^+/$PDCN_X$/GCE on the decrease of DPV peak current.

washing. As can be seen in Figure 5B, the Δi_p values were linear with the logarithmic value of captured cell numbers in the range of 200 to 9800 with a correlation coefficient of 0.99. The linear regression equation was

$$\Delta i_p = -1.0 + 6.14 \log n \quad (1)$$

On the other hand, after partly blocking the mannose-specific binding sites on the cytosensor, the Ab_2-HRP/Ab_1/HeLa/Con A/AuNPs/TH^+/$PDCN_X$/GCE showed a higher DPV peak current in 0.1 M pH 7.4 PBS containing 10.0 mM H_2O_2 (curve b in Figure 6A) than that obtained without blocking (curve c in Figure 6A). That is to say, the electrocatalytic peak current (Δi_p) decreased upon the blocking. The decrease of Δi_p ($\Delta i_p'$) was related to the mannosyl sites on the uncaptured cells surfaces, which could be expressed as the amount of mannose (m) used to block Con A. Figure 6B displayed the plots of $\Delta i_p'$ versus the amount of mannose used for blocking. Each point on the calibration curve corresponded to the mean value obtained from three independent measurements. The $\Delta i_p'$ was proportional to the logarithmic value of the mannose numbers ranging from 0.125 to 2.0 pmol with a correlation coefficient of 0.98. The linear regression equation was

$$\Delta i_p' = -5.56 - 2.80 \log m \text{ (pmol)} \quad (2)$$

Meanwhile, the $\Delta i_p'$ could be converted into the number of uncaptured cells according to eq 1. Thus, the mannosyl sites on each uncaptured HeLa cell could be calculated from eqs 1and 2 to correspond to about $(4 \pm 2) \times 10^{10}$ molecules of mannose moieties.

Additionally, the proposed cytosensor was also used for the evaluation of P-gp on the HeLa cell surface. As mentioned above, the Δi_p showed a linear relationship with the concentration of Ab_1 ranging from 2.0 to 10.0 $\mu g\ mL^{-1}$ used for incubation. The linear regression equation was

$$\Delta i_p = 9.28 + 1.14 C_{Ab1} \ (\mu g\ mL^{-1}) \quad (3)$$

On the basis of the specific recognition between P-gp on the cell surface and Ab_1, a method was then designed by preincubating the HeLa cells with a certain amount of Ab_1 for 1 h. After centrifugation, the supernatant was carefully collected and used for the incubation with HeLa/Con A/AuNPs/TH^+/$PDCN_X$/GCE. Because of the difference of Δi_p, the amount of Ab_1, which has been bound to the surface of HeLa cells during the preincubation, was calculated as 9.57×10^{-2} μg according to eq 3. On the other hand, the number of HeLa cells used for preincubation could be determined using a Petroff-Hausser cell counter. Therefore, the amount of glycoprotein on each HeLa cell could be calculated correspondingly to about 8.47×10^6 molecules.

CONCLUSIONS

The present study describes the first application of nitrogen-doped carbon nanotubes in the construction of cell-based electrochemical immunoassay. The cytosensor applied a novel 3-D architecture of $PDCN_X$/TH^+/AuNPs for stable immobilization of Con A for selective recognition of the cell surface carbohydrates. By combination of the advantages of 3-D architecture, enzyme amplification, and electrochemical measurement, the proposed cytosensor showed a wide linear range and low detection limit for quantification of HeLa cells. Moreover, the method presented herein exhibited the capability of evaluating the cell surface carbohydrates and P-glycoprotein. We therefore predict that this designed strategy can also be extended to other carbohydrate and lectin recognition events and thus provides an avenue for evaluating the expression profiles of cell surface carbohydrates and revealing the functions of carbohydrates in underlying biological processes related to cancers.

ACKNOWLEDGMENT

We greatly appreciate the support of the National Natural Science Foundation of China for the Key Program (Grant 20635020) and the Creative Research Group (Grant 20821063). This work is also supported by National Basic Research Program of China (Grant 2006CB933201). The authors thank the kind help from Professor Zheng Hu, Key Laboratory of Mesoscopic Chemistry of MOE and School of Chemistry and Chemical Engineering, Nanjing University.

SUPPORTING INFORMATION AVAILABLE

Additional information as noted in text. This material is available free of charge via the Internet at http://pubs.acs.org.

Received for review November 14, 2009. Accepted March 27, 2010.

AC9026127